AD_____

Award Number: W81XWH-11-1-0184

TITLE: The Mechanism by which Neurofibromin Suppresses Tumorigenesis

PRINCIPAL INVESTIGATOR: Wei Mo

CONTRACTING ORGANIZATION: University of, Southwestern Medical Center at Dallas, Dallas, TX, 75239

REPORT DATE: February 2013

TYPE OF REPORT: Annual Summary

PREPARED FOR: U.S. Army Medical Research and Materiel Command
Fort Detrick, Maryland 21702-5012

REPORT DOCUMENTATION PAGE

Form Approved
OMB No. 0704-0188

1. REPORT DATE	2. REPORT TYPE	3. DATES COVERED
February 2013	Annual Summary	1 February 2011- 31 January 2013

4. TITLE AND SUBTITLE
The Mechanism by which Neurofibromin Suppresses Tumorigenesis

5a. CONTRACT NUMBER

5b. GRANT NUMBER
W81XWH-11-1-0184

5c. PROGRAM ELEMENT NUMBER

6. AUTHOR(S)
Wei Mo

5d. PROJECT NUMBER

5e. TASK NUMBER

5f. WORK UNIT NUMBER

7. PERFORMING ORGANIZATION NAME(S) AND ADDRESS(ES)
University of, Southwestern Medical Center at Dallas, Dallas, TX, 75239

8. PERFORMING ORGANIZATION REPORT NUMBER

9. SPONSORING / MONITORING AGENCY NAME(S) AND ADDRESS(ES)
U.S. Army Medical Research and Materiel Command
Fort Detrick, Maryland 21702-5012

10. SPONSOR/MONITOR'S ACRONYM(S)

11. SPONSOR/MONITOR'S REPORT NUMBER(S)

12. DISTRIBUTION / AVAILABILITY STATEMENT
Approved for Public Release; Distribution Unlimited

13. SUPPLEMENTARY NOTES

14. ABSTRACT
Malignant Peripheral Nerve Sheath Tumors (MPNSTs) are soft tissue sarcomas that arise in connective tissue surrounding peripheral nerves. They occur sporadically and in a subset of patients with Neurofibromatosis type-1 (NF1) syndrome. MPNSTs are highly aggressive,therapeutically resistant, and typically fatal. Using comparative transcriptome analysis, we identified CXCR4, a G protein-coupled receptor, as highly expressed in mouse models of NF1-deficient MPNSTs, but not in non-transformed precursor cells. In MPNSTs, high chemokine CXCR4 receptor and CXCL12 ligand levels promote tumor growth by stimulating cyclin D1 expression and cell cycle progression through PI3-kinase (PI3K) and β-catenin signaling. Suppression of CXCR4 activity, either by shRNA or pharmacological inhibition decreases MPNST cell growth in culture and inhibits tumorigenesis in allografts and in spontaneous genetic mouse models of MPNST. We further demonstrate conservation of these activated molecular pathways in human MPNST. Taken together, our findings indicate a role for CXCR4 in NF1-associated MPNST development, and identify a novel therapeutic target.

15. SUBJECT TERMS- MPNST, CXCR4, CXCL12, Cyclin D1

16. SECURITY CLASSIFICATION OF:			17. LIMITATION OF ABSTRACT	18. NUMBER OF PAGES	19a. NAME OF RESPONSIBLE PERSON
a. REPORT	b. ABSTRACT	c. THIS PAGE			USAMRMC
U	U	U	UU		19b. TELEPHONE NUMBER *(include area code)*

Table of Contents

28 Pages

Introduction

The tumor predisposition disorder von Recklinghausen's Neurofibromatosis type I (NF1) is one of the most common genetic disorders of the nervous system, affecting 1 in 3500 individuals worldwide (Zhu, 2001). A cardinal feature of NF1 is the growth of benign tumors called neurofibromas, categorized into plexiform and dermal subtypes (Le, 2007). Plexiform neurofibromas can undergo malignant transformation into neurofibrosarcomas, known as malignant peripheral nerve sheath tumors (MPNSTs), which represent a major source of morbidity for NF1 patients (Ferner, 2007). Despite continued progress in understanding NF1 biology, MPNST treatment remains limited to surgery, and prognosis remains unchanged (Tonsgard, 2006).

The development of murine models has provided an opportunity to gain insight into NF1-deficient tumor natural history (Cichowski et al., 1999; Joseph et al., 2008; Vogel et al., 1999; Zheng et al., 2008; Zhu et al., 2002). *NF1* and *TP53*, or *CDKN2a*, are the most frequently mutated cancer-related genes in human MPNSTs (Mantripragada et al., 2008; Rubin and Gutmann, 2005). Our genetically-engineered mouse models (GEMMs) recapitulate tumors that arise in NF1 patients, and we and others have shown that genetic ablation of the *NF1* and *p53* tumor suppressors results in spontaneous development of MPNSTs (Cichowski et al., 1999; Vogel et al., 1999). Benign and malignant *Nf1*-deficient tumors can also be induced by subcutaneous implantation of *Nf1* or *Nf1;p53* deficient skin-derived precursor (SKPs) respectively, and are histologically indistinguishable from human counterparts (Le et al., 2009); unpublished observations).

Here, we examine the chemokine receptor CXCR4, which we find enriched in *Nf1*-deficient cells, and particularly in *Nf1*-deficient MPNSTs. Expression of CXCR4 and its ligand,

CXCL12, has been reported in solid tumors, (Kijima et al., 2002; Koshiba et al., 2000; Laverdiere et al., 2005; Muller et al., 2001; Oh et al., 2001; Righi et al., 2011; Schrader et al., 2002; Sehgal et al., 1998; Sengupta et al., 2011; Taichman et al., 2002; Zeelenberg et al., 2003; Zhou et al., 2002), as well as non-Hodgkin's lymphoma (Bertolini et al., 2002), and chronic lymphocytic leukemia (Burger et al., 1999). Clinical data indicate that high CXCR4 correlates with poor clinical outcome (Bian et al., 2007; Li et al., 2004; Wang et al., 2008). The proposed paracrine roles for CXCR4/CXCL12 in a variety of tumorigenic processes include cell growth (Schrader et al., 2002; Zhou et al., 2002), metastasis (Li et al., 2004), and angiogenesis (Sengupta et al., 2011).

A potential role for CXCR4 in sarcoma pathogenesis, however, has not been examined. Here, we provide evidence that the CXCR4/CXCL12 axis is essential for MPNST tumor progression. Specifically, the autocrine activation of CXCR4 by CXCL12 triggers intracellular PI3K and β-catenin signals to promote G1 to S phase transition in MPNST cells. The CXCR4 antagonist, AMD3100, has growth-inhibitory effects on primary cultured mouse and human MPNST cells, tumor allografts, and spontaneous GEMMs. Moreover, analysis of human primary and cultured MPNST cells, as well as human tissue microarray analysis, reveals conserved pathway activation. Thus, CXCR4 inhibition may represent a new therapeutic strategy to treat MPNST.

Body

Key Research Accomplishments

• CXCR4 and CXCL12 expression is elevated in murine and human MPNST cells and tumors

• CXCR4 depletion inhibits MPNST proliferation by down-regulating cyclin D1

• CXCR4 promotes tumorigenesis through the AKT/β-catenin signaling pathways

• Pharmacologic inhibition of CXCR4 blocks allograft and spontaneous tumor formation

Reportable Outcomes

CXCR4 in *NF1*-deficient MPNST tumors.

Previously, we demonstrated that *Nf1*-deficient SKPs can give rise to either dermal or plexiform neurofibromas depending on their local microenvironment (dermis vs. sciatic nerve) (Le et al., 2009). In addition, dual mutation of the *Nf1* and *p53* tumor suppressors in these cells results in MPNSTs that exhibit cellular and molecular features of human MPNSTs (LQL & LFP, unpublished observations). These tumors are indistinguishable from a spontaneous MPNST GEMM also based on loss of *Nf1* and *p53* (cis*NP*; Cichowski et al., 1999; Vogel et al., 1999). To gain insight into the molecular and cellular mechanisms underlying development of *Nf1*-deficient MPNSTs, we used microarray analysis to compare the transcriptomes of MPNSTs with those of normal SKPs (WT), as well as pre-tumorigenic SKPs with either *Nf1* deletion (*Nf-/-*) or *Nf1* and *p53* (*NP-/-*) deletion as shown in Figure 1A. The comparative array data presented a complex picture of up- and down-regulated transcripts for diverse genes (data not shown). However, our attention was drawn to the elevated expression of the chemokine receptor CXCR4 that exhibited a three-fold elevation in both pre-tumor cell types (*Nf-/-*; *NP-/-*), and a twelve-fold increase in the malignant form of SKP MPNST (SMPNST). Quantitative RT-PCR and western blot analysis

(Figure 1B and 1C) confirmed these array data. We also measured low CXCR4 levels in Schwann cells, which belong to the embryonic lineage of origin of *NF1*-deficient tumors (Le et al., 2011; Serra et al., 2000; Zhu et al., 2002), and high levels in tumor cells from the spontaneous cis*NP* mouse model of MPNST by western blot (Figure S1A; (Vogel et al., 1999) and immunohistochemistry (IHC). We further performed IHC on tumor samples from the SMPNST-allograft, cis*NP*, and SMPNST-autograft models, and a human MPNST sample (Figure 1D and S1B). Together, these data confirmed elevated CXCR4 protein in the different sources of *Nf1*-deficient malignant tissues compared to controls and, further, provided evidence that CXCR4 expression is sustained in human *NF1*-associated MPNST.

CXCR4 knockdown impairs cell proliferation and attenuates tumorigenesis.

To evaluate the functional role of CXCR4 in MPNST pathogenesis, we used shRNA for knockdown in SMPNST cells. Cells were infected with lentivirus containing CXCR4 shRNA or a control scrambled shRNA (pLKO ctrl), and stable cell lines were established using puromycin selection. Two different shRNA sequences, targeting either the coding region (pLKO-mCXCR4) or the 3' UTR (pLKO-mCXCR4-UTR) reduced CXCR4 mRNA levels by approximately 90% (Figure S2A and S2B). To address whether CXCR4 influences SMPNST cell metabolism, we measured ATP levels using a luminescence assay, and found that tumor cells with depleted CXCR4 were less metabolically active. Introduction of exogenous CXCR4 cDNA lacking the UTR sequences, and so not targeted by the shRNA, re-established CXCR4 protein levels and overcame the cell growth inhibition (Figure 2A and S2B).

We turned to a doxycycline (dox)-inducible Mir30-based shRNA system to enable acute knockdown of CXCR4. Using this system, murine and human CXCR4 mRNA levels were decreased to 25% and 10% of the origin level, respectively (Figure S2C-F). In contrast, induction with dox had no effect on CXCR4 expression in MPNST-Tripz-scrambled control cells (Figure

S2C-F). Similar to the pLKO knockdown results, we observed cell growth arrest in CXCR4-depleted SMPNST and human MPNST (S462) cells upon dox treatment (Figure 2B). Together, these results confirm that CXCR4 plays a role in murine- and human-derived MPNST cell proliferation.

We next investigated the growth properties of tumor cells *in vivo* after CXCR4 knockdown. 10^4 or 10^5 pLKO-mCXCR4 or pLKO-ctrl SMPNST cells were injected subcutaneously into nude mice and monitored for tumor growth (SMPNST-allografts). One month after injection, the mice were sacrificed and tumors dissected (Figure S2G). Quantification of tumor size and weight showed that MPNST cells with CXCR4 knockdown generated smaller tumors than control cells (Figure S2H), and additionally, time to tumor appearance was significantly increased (Figure S2I). We also analyzed cell proliferation in excised tumors and found the average percentage of Ki67-positive, proliferating cells was 24.2 ± 6.5% in CXCR4-depleted MPNSTs versus 67.6 ± 5.1% in controls (Figure S2J and S2K).

Similar results were obtained when the inducible shRNA tumor cells were implanted and subjected to dox-mediated CXCR4 knockdown after the tumor cells had successfully seeded in the allograft. This approach eliminated the possibility that CXCR4 knockdown in culture impeded subsequent tumor cell implantation. 10^4 or 10^5 MPNST-Tripz-CXCR4 cells were injected subcutaneously into nude mice and one group received dox (1 mg/ml) in the drinking water (Figure 2C). Compared to controls, tumor appearance in the dox-treated group was delayed by one week and tumor progression was impaired (Figure 2C and 2D). All mice were sacrificed on Day 26 and tumors were excised. Western blot analysis showed a ~73.1% depletion of CXCR4 protein in the tumors harvested from dox-treated mice (Figure 2E). When 10^5 cells were injected, 6/6 control mice bore tumors (759 ± 500 mm^3 in size and 0.467 ± 0.226 gram in weight) and 5/6 dox-treated mice developed tumors that were smaller both in size (199 ± 115

mm^3) and weight (0.1± 0.08 gram) (Figure 2F and 2G). Notably, when 10^4 cells were injected, no dox-treated mice developed tumors, while control group mice developed tumors (Figure 2D). Thus, both chronic and acute suppression of CXCR4 *in vivo* substantially decreased the tumorigenic capacity of MPNST cells.

CXCR4 depletion alters the MPNST cell cycle.

We investigated possible mechanisms of CXCR4 function in promoting MPNST progression. shRNA depletion caused growth arrest of SMPNSTs (Figure 2) rather than apoptosis (Figure S3A and S3B) or senescence (Figure S3C and S3D). Bromodeoxyuridine (BrdU) incorporation and FACS analysis showed significant reduction in BrdU incorporation in CXCR4-depleted cells (57.2 ± 3.6% versus 21.8± 2.6%; Figure 3A). When CXCR4 protein level was restored, the percentage of BrdU-positive cells was also restored to that of CXCR4-WT cells (Figure 3A). Additional cell cycle analysis revealed the percentage of cells in G1 phase was ~60% in CXCR4-depleted SMPNST cells versus ~25% in CXCR4-WT cells; by contrast, the number of cells in G2/M phase was only slightly changed (Figure 3B and S3E). These data suggest that CXCR4-depleted MPNST cells undergo G1/S arrest. We also performed BrdU incorporation studies *in vivo*. Tumor-bearing mice were injected with BrdU three hours before sacrifice. BrdU IHC revealed 42 ± 11% BrdU-positive cells in the tumor samples from mice injected with control SMPNST cells. In contrast, the BrdU-positive cell number decreased to 15 ± 5% in the tumor samples from mice injected with CXCR4-depleted SMPNST cells (Figure 3C and 3D). Similar to the MPNST cell culture results, there was no obvious apoptosis in either tumor group (Figure S3F and S3G). In summary, knockdown of CXCR4 expression, in culture and *in vivo*, led to cell cycle arrest manifested by reduced S phase and BrdU incorporation, rather than cell death or senescence.

Cyclin D1 expression is regulated by CXCR4.

We next investigated whether CXCR4 perturbation impacts the expression of cell-cycle-regulatory genes (Johnson and Walker, 1999; Lee and Yang, 2003; Obaya and Sedivy, 2002). While qRT-PCR analysis indicated that expression of most genes examined was unchanged in CXCR4-depleted SMPNST cells and tumors, cyclin D1 mRNA levels decreased ~70% (Figure 3E and S3H). A slight reduction in CDK4/6 and cyclin E mRNA levels was also observed (Figure 3E and S3H). Quantification of western blots confirmed the cyclin D1 protein level decrease in CXCR4-depleted MPNST cells and tumors (SMPNST-allografts) (Figure 3F and S3I). Both cyclin D1 mRNA and protein levels were fully restored in CXCR4-depleted MPNST cells with exogenous CXCR4 expression (Figure 3E and 3F). Moreover, reintroduction of cyclin D1 cDNA restored protein levels and counteracted the CXCR4 depletion effect, allowing cells to resume progression through the cell cycle (Figure 3G and 3H). These data demonstrate that in SMPNST cells, cell cycle progression mediated by cyclin D1 is dependent on CXCR4 function.

CXCR4 activates the AKT/GSK-3β/β-catenin network

Signaling pathways known to regulate cyclin D1 include the NFκB, Ras, ERK, Wnt/β-catenin and JAK/STAT3 pathways (Sherr, 1995). To determine whether any of these candidate pathways mediate CXCR4 regulation of cyclin D1 in neurofibrosarcomas, fractionated nuclear and cytoplasmic extracts of SMPNST cells were immunoblotted with the indicated antibodies to examine changes following CXCR4 depletion. We observed that both cyclin D1 and β-catenin levels decreased 76.4% and 77.3%, respectively, in the nuclear fraction of CXCR4-depleted MPNST cells (Figure 4A). No changes were seen in other pathways examined (Figure 4A).

Transcriptional activation assays using a luciferase reporter linked to the TCF promoter - a physiological target of β-catenin - showed a 57% reduction in luciferase activity in CXCR4-depleted SMPNST cells compared to controls, consistent with the model that suppression of CXCR4 attenuated β-catenin activity (Figure 4B). To test whether nuclear β-catenin is required for cyclin D1 expression, we directly blocked TCF function (Hoppler and Kavanagh, 2007). Expression of dominant-negative TCF (dnTCF) dramatically decreased cyclin D1 mRNA and protein levels in CXCR4-WT-MPNST cells (Figure 4C and 4D), while over-expression of β-catenin in CXCR4-depleted MPNST cells restored cyclin D1 expression (Figure 4E) and further, rescued the cell growth arrest caused by CXCR4 knock down (Figure 4F). Functionally, down regulation of the β-catenin pathway by dnTCF resulted in cell growth arrest in MPNST cells (Figure S4A). We also examined tumors for β-catenin expression. IHC on MPNST tumor tissues from SMPNSTs (SMPNST-allografts) (Figure S4B) and one human patient sample (Figure S4C) showed robust nuclear immunoreactivity consistent with activation of β-catenin signaling in these tumors.

The above data demonstrate a role for β-catenin downstream of CXCR4, and upstream of TCF and cyclin D1 in stimulating MPNST growth. β-catenin stabilization is required for its role as a transcription factor. In the inactive state, β-catenin is destabilized by phosphorylation at Ser33, Ser37, and Thr41 by GSK-3β, or at Ser45 by CK1α (Liu et al., 2002) Western blot analysis showed that CXCR4 depletion increased β-catenin serine phosphorylation at sites 33/37 but not 45 (Figure 4G), suggesting that CXCR4 suppression resulted in GSK-3β kinase activation. We also examined GSK-3β serine 9 inactivating phosphorylation and observed a reduction in CXCR4-depleted MPNST cells (Figure 4G). Thus, in MPNST, CXCR4 activity maintains GSK-3β in the inactive state. GSK-3β is in turn, a downstream element of the PI3K/AKT signaling pathway (Cross et al., 1995) whose kinase activity is inhibited by AKT-

mediated phosphorylation at Ser9 (Srivastava and Pandey, 1998). We reasoned that the decreased phosphoSer9-GSK-3β level in CXCR4-depleted MPNST cells might result from attenuated AKT kinase activity, and confirmed this by western blot analysis with pAKT (Ser473) antibody (Figure 4G). We also found reduced levels of activated β-catenin, pGSK-3β (Ser9) and pAKT (Ser473) in CXCR4-depleted MPNST tumor samples compared to control tumors (SMPNST allografts) (Figure 4H). These data support the model that CXCR4 promotes MPNST growth by activating the PI3K/AKT and the GSK-3β/β-catenin pathways. Previous *in vitro* studies using human and murine MPNST cell lines, as well as *in vivo* studies using the cis*NP* mouse model demonstrated that the mTOR pathway can regulate MPNST growth by post-transcriptional regulation of cyclin D1 (Johannessen et al., 2008). We observed modest reduction in phospho-mTOR upon CXCR4 knockdown but this was not accompanied by obvious change in the levels of phosphorylated-S6 ribosomal protein (Figure S4D). Collectively, our data indicate that CXCR4 regulates the activity of β-catenin via the AKT/GSK-3β cascade, which ultimately controls cyclin D1 transcription and protein levels.

CXCL12 activates CXCR4 in an autocrine loop.

We sequenced CXCR4 cDNAs from two independent murine MPNSTs, one derived from the SMPNST-allograft model and one from the cis*NP* model, and found no missense or nonsense mutations (data not shown). Moreover, CXCR4 activating mutations have not been identified in MPNST cell lines or primary cells derived from human patients (see below and Figure S5A). Therefore, in these tumors, receptor activity must rely on the presence of ligand: CXCL12. qPCR analysis showed that CXCL12 mRNA was indeed elevated in pretumorigenic SKPs (*NP-/-*) and even more highly expressed in SMPNST tumor cells (Figure S5B). To test the role of CXCL12 in MPNST cell growth, we treated cultured MPNST cells with recombinant CXCL12 protein and found that it promoted cell growth, generating a 1.5-fold increase in cell number at a

concentration of 10 ng/ml by Day 6, when compared to non-treated cells (Figure 5A). In contrast, cell number decreased by 25% and 55% at day 3 and 6, respectively, when cells were cultured with anti-CXCL12 antibody compared to IgG or PBS control (Figure 5B). These data suggest that CXCL12 is critical for MPNST cell proliferation. To verify the autocrine source of CXCL12 ligand in the MPNST cell culture, we performed an ELISA on the medium conditioned by MPNST cells using an anti-CXCL12 antibody. We observed no detectable CXCL12 protein in control media (with no cells) compared to the conditioned media, indicating that the *in vitro* source of CXCL12 protein is the MPNST cells (Figure 5C). Consistent with the ELISA showing that conditioned media from CXCL12-overexpressing MPNST cells (pBabe-CXCL12), and knockdown cells (pLKO-CXCL12) contained elevated and reduced cytokine, respectively (Figure 5C and S5C), CXCL12-overexpressing cells had a significant growth advantage (Figure 5A), while CXCL12 knockdown cells exhibited a significant reduction in growth at Day 3 and Day 6 (Figure 5D). Importantly, the cell growth inhibition could be rescued by addition of CXCL12 protein (Figure 5E). Therefore, MPNST cells synthesize and secrete CXCL12 protein causing increased cell growth that corresponded with CXCL12 levels. To confirm that the effect of CXCL12 on MPNST growth is dependent on CXCR4, we added CXCL12 protein to cultured CXCR4-depleted MPNST cells. We found no detectable change in cell proliferation after ligand stimulation compared to control CXCR4-depleted MPNST cells (Figure 5E). Additionally, CXCL12 modulation in the presence of receptor induced the same signaling pathway changes brought about by CXCR4 modulation (Figure 5F). Taken together, these data demonstrate that CXCL12, secreted by MPNST cells, is sufficient to sustain autocrine activation of its receptor, CXCR4, and triggers specific downstream signaling pathways, leading to MPNST cell cycle progression and proliferation.

Given the important roles of CXCR4/CXCL12 in tumor angiogenesis, we also investigated whether CXCR4 depletion in MPNST cells altered the microvasculature. Both control and CXCR4-depleted tumors exhibit strong CD31 staining (Figure S5D) and similar vessel densities (Figure S5E), indicating that the tumor growth arrest induced by CXCR4 depletion is cell autonomous and not secondary to effects on the microvasculature.

Pharmacological inhibition of CXCR4 arrests MPNST proliferation and tumor growth.

We next tested a clinically validated, highly specific CXCR4 antagonist, AMD3100, in our system. We performed a dose-response analysis of AMD3100 on primary murine MPNST cells (SMPNSTs and cis*NP*), one primary human MPNST cell line, three established human MPNST cell lines (S462; SNF02.2; SNF96.2), and pre-tumor cells (*NF;p53* null SKPs) (Figure 6A and 6B). Four of six cell lines were potently inhibited by low doses of AMD3100 (IC50 values$\leqq$0.5 uM; Figure 6C). One human MPNST cell line, SNF96.2, and the pre-tumor cells were less sensitive (IC50 values of 1-10 uM; Figure 6C). Only one human MPNST cell line, SNF02.2, showed no response, consistent with its low endogenous CXCR4 levels relative to the other MPNST cells (Figure S6A). Of note, we were unable to seed xenograft tumors using SNF02.2 cells suggesting that this cell line has drifted significantly from the original tumor of derivation (data not shown). In contrast, the cell viability of wild-type Schwann cells and SKPs was unaffected by AMD3100 (Figure 6A). Inhibition of CXCR4 by AMD3100 also reduced cyclin D1 levels via the AKT/GSK-3β/β-catenin pathway (Figure 6D).

To assess the therapeutic potential of AMD3100 *in vivo*, we first tested subcutaneous allografts of primary SMPNSTs. Transplant recipient animals with palpable tumors were treated with AMD3100, and after three weeks of treatment were sacrificed for analysis (Figure 6E). AMD3100 treatment potently suppressed MPNST growth, resulting in reduced tumor size and

weight that was 38% and 42%, respectively, of the control group (Figure S6B). This was accompanied by commensurate reduction in BrdU incorporation and Ki67 staining (Figure S6C and S6D). Consistent with the *in vitro* data, AMD3100-treated tumors showed decreased levels of cyclin D1, activated β-catenin, phospho-AKT, and phospho-ser9-GSK-3β (Figure S6E).

To further validate the role of CXCR4 signaling in MPNST growth and the potent cytostatic effect of AMD3100 on tumor growth, we turned to a spontaneous endogenous GEMM. A mouse strain in which null *p53* and *NF1* alleles are configured in *cis,* on the same chromosome, spontaneously develop MPNST via loss of heterozygosity (LOH) of both tumor suppressor alleles (*cisNF/p53*; Vogel et al., 1999). While a majority of the spontaneous tumors are sarcomas, these *cisNF/p53* mice are also prone to other NF1-initiated tumors such as lymphomas and gliomas, as well as to spontaneous p53-based tumors (Cichowski et al., 1999; Vogel et al., 1999; Reilly et al., 2004). Based on Kaplan-Meier curve data that indicate spontaneous neurofibrosarcoma appearance with 20% mortality at about 15 weeks of age and 70 percent mortality at 25 weeks (N=170; Vogel et al., 1999), we commenced the AMD3100 drug trial on *cisNF/p53* mice at 16 weeks of age. As shown in Figure 6F, at two months post treatment (24 weeks of age), 7/10 control mice (70%) had perished whereas in the AMD3100 group, only 3/17 (18%) had perished. All perished mice had large tumors and histopathological analysis of the tumor tissue revealed that one mouse from the control group and one from the experimental group had clear evidence of a primary tumor of hematopoietic origin (Figure S6F and S6G). Therefore, these mice were removed from the study resulting in a total of 9 control mice and 16 AMD3100-treated mice (Fig. 6G). Six out of nine control mice developed lethal sarcomas. Five developed MPNST, as evidenced by histopathological analysis, and S100β and GAP43 immunoreactivity (Figure 6F: C1, C2, and C5-C7; Figure S6H). A sixth control mouse died with a malignant triton tumor (MTT), sarcomatous NF1-associated tumors with high myoglobin

expression (Figure 6F: C4; and Figure S6I). All six tumors displayed CXCR4 expression (Figure 6F). In contrast to the high mortality rate in the control group, at two months post-treatment, only two out of sixteen mice from the AMD3100 treatment group had perished with a solid tumor (Figure 6F: AMD1 and AMD3; Figure 6G). By histological analysis, we determined that one of the tumors was a rhabdomyosarcoma (RMS), with very low levels of CXCR4 expression (Figure 6F: AMD3, and Figure S6J and S6K). The second treated mouse developed a leiomyosarcoma (LMS), with CXCR4 expression (Figure 6F: AMD1, and Figure S6L and S6M) suggesting that this tumor escaped AMD3100 treatment. Whether this outlier reflects failed drug delivery, or alternatively, an independent mechanism of tumor promotion will require additional studies.

In summary, the allograft and genetic tumor model data demonstrate that *in vivo* pharmacological blockade of CXCR4 can potently inhibit spontaneous MPNST tumor development by blocking the same signaling pathways as observed in primary tumor cultures.

Conserved signaling pathway activation in human MPNST.

The above studies reflect analyses of genetic mouse models extended to a single human tumor and primary MPNST line plus three established human MPNST lines. To further assess the relevance of our findings to human MPNST, we examined CXCR4 in MPNSTs from patients with NF1. We sequenced the coding exons (1 & 2) of CXCR4 in eleven NF1-associated human MPNST samples (Figure S5A): four MPNSTs, two primary cultures, and five MPNST cell lines including S462, which requires CXCR4 function for growth (Figure 6B); all CXCR4 coding regions had wild-type sequence (Figure S5A). Thus, similar to the murine MPNSTs, human MPNST CXCR4 activity must depend on ligand presence. We next examined CXCR4 protein expression using a human tissue microarray (TMA) that included seventeen plexiform neurofibromas (from NF1 patients harboring MPNSTs) and seventy-three MPNST samples

(forty-three from NF1 patients and thirty sporadic) (Ghadimi et al., 2012; Zou et al., 2009). The data showed that 94% of neurofibromas and 98% of NF1-deficient MPNSTs displayed CXCR4 immunoreactivity (Figure 7A and 7B), while only 66% of sporadic MPNSTs tissues showed CXCR4 immunoreactivity. Similarly, 71% of neurofibromas and 77% of NF1-associated MPNSTs exhibited CXCR4 expression in >5% of tumor cells as compared to 40% of sporadic MPNST tissues (Figure 7A). Spearman correlation analysis showed a statistically significant difference in CXCR4 intensity and distribution when comparing NF1-associated to sporadic tumors ($p=0.0012$ and 0.0008, respectively) (Figure 7B). We also assessed p-AKT, β-catenin and cyclin D1 expression and observed a direct concordance between their levels and those of CXCR4 ($p=0.0198$, 0.0028 and 1.93E-04, respectively) (Figure 7C and 7D). Thus, TMA data confirm that AKT/GSK-3β̃/β-catenin pathway activation is conserved in human NF1-associated MPNSTs. Extension of our functional data in murine and human MPNST cells, coupled with the TMA studies, indicate that CXCR4 and cyclin D1 are closely associated with clinical NF1-associated pathogenesis.

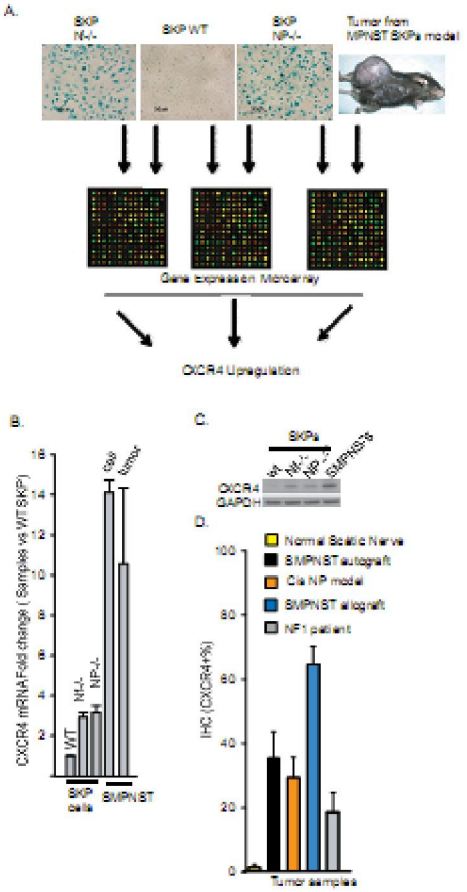

Figure 1. CXCR4 is overexpressed in MPNSTs. (A) Schema of the microarray analyses.
(B) qRT-PCR analysis of CXCR4 mRNA levels in WT, *Nf-/-* and *NP-/-* (*Nf-/-;p53-/-*) SKPs, as well as MPNST SKP model tumors and the cells derived from the tumor. (C) Western blot analysis of CXCR4 protein levels in *Nf-/-* and *NP-/-* SKPs, and SMPNST cancer cells. (D) Quantification of CXCR4-positive cells in tumor tissues from different mouse models of MPNST and an MPNST from an NF1 patient (SMPNST = SMPNST autograft; athymic model = SMPNST allograft). All statistics represent mean ± SD.

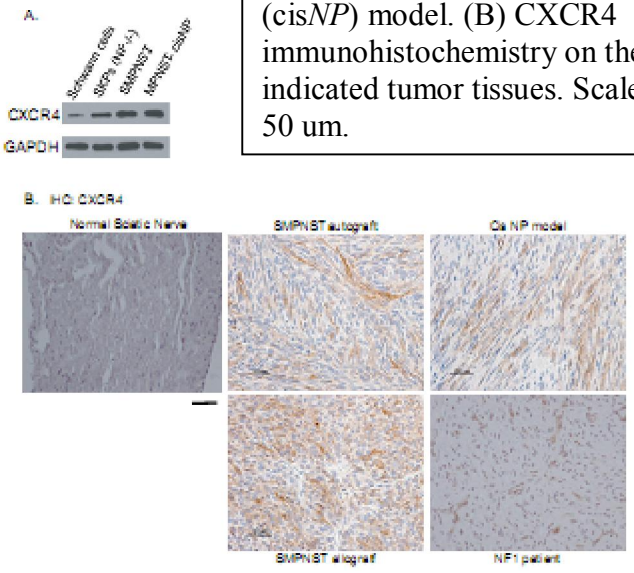

Figure S1. (A) Western blot analysis of CXCR4 protein levels in Schwann cells, SKPs (NP null = *Nf-/-;p53-/-*) and MPNST cells isolated either from the MPNST SKP model or the cis*Nf/p53* (cis*NP*) model. (B) CXCR4 immunohistochemistry on the indicated tumor tissues. Scale bar: 50 um.

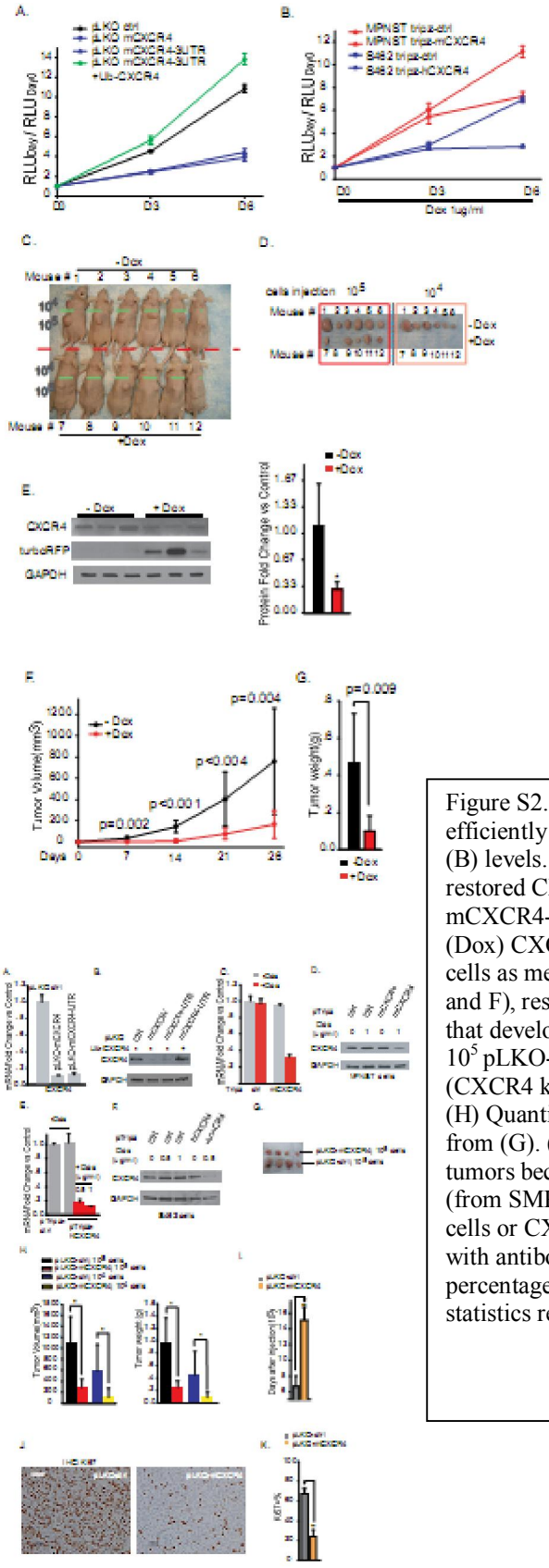

Figure 2. Knockdown of CXCR4 expression in MPNST cells decreased proliferation in vitro and tumorigenesis in vivo. (A and B) ATP luminescence assays were used to measure growth of indicated cells. (C and D) Representative pictures of the tumors from nude mice injected with SMPNST-Tripz-mCXCR4 cells. Mice #1-6: without Dox treatment; Mice #7-12: Dox treatment. (E) CXCR4 protein level is down-regulated in dox-treated MPNSTs. (F) Kinetic curve of tumor growth as measured by tumor volume. (G) Quantification of tumor weight. All statistics represent mean ± SD.

Figure S2. Two different pLKO-mCXCR4 shRNAs efficiently knock down CXCR4 mRNA (A) and protein (B) levels. Ectopic CXCR4 expression (Ub-CXCR4) restored CXCR4 protein levels in SMPNST-pLKO-mCXCR4-UTR cells (B). (C-F) Doxycycline–induced (Dox) CXCR4 depletion in both SMPNST cells and S462 cells as measured by qPCR (C and E) and western blot (D and F), respectively. (G) Representative picture of tumors that developed in nude mice injected subcutaneously with 10^5 pLKO-ctrl (control) cells or pLKO-mCXCR4 (CXCR4 knockdown) cells (SMPNST-allograft tumors). (H) Quantification of the size and weight of the tumors from (G). (I) Graph showing days after injection that tumors became palpable. (J) Paraffin sections of MPNSTs (from SMPNST-allografts - injection of control SMPNST cells or CXCR4-depleted SMPNST cells) were stained with antibody against Ki67. (K) Quantification of the percentage of Ki67-positive cells. Scale bar: 50 um. All statistics represent mean ± SD. (*p< 0.05; **p< 0.01).

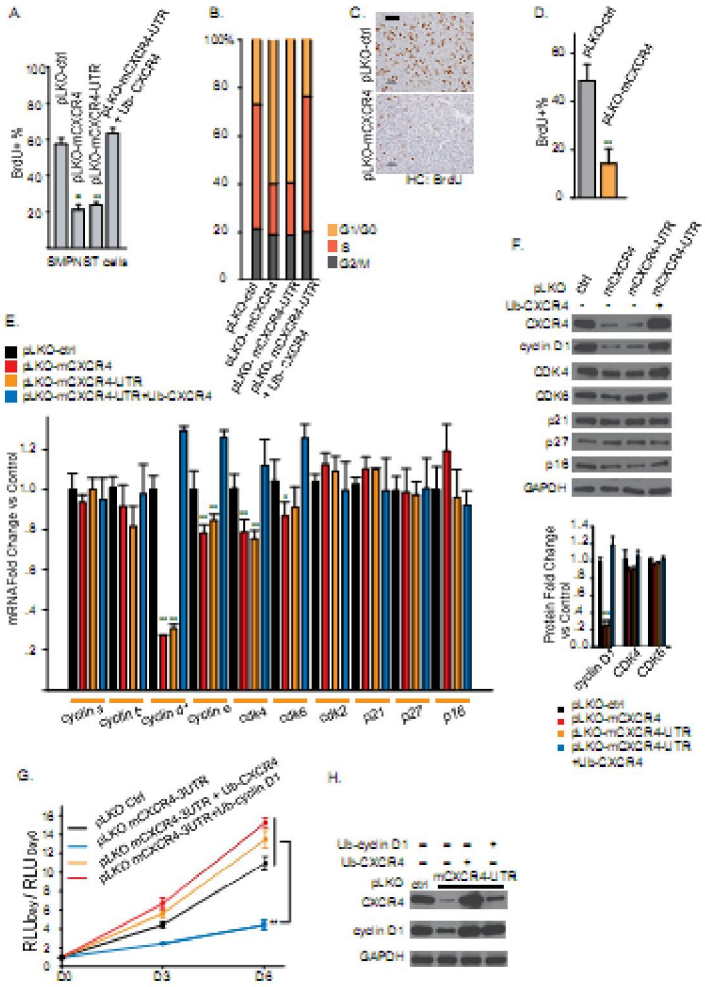

Figure 3. CXCR4 alters the cell cycle in SMPNST cells by regulating cyclin D1 expression. SMPNST cells were incubated with BrdU for 30 min and then stained with propidium iodide. (A and B) FACS analysis showed that CXCR4 depletion in SMPNST cells decreased the percentage of BrdU-positive cells (pLKO-mCXCR4 and pLKO-mCXCR4-UTR compared to control pLKO-ctrl) (A) and altered the proportion of cells in G1 and S phase (B). Expression of CXCR4 in the knockdown cells (pLKO-mCXCR4-UTR + Ub-CXCR4) restored the cells to the control state. (C) Paraffin sections of MPNSTs (harvested from SMPNST-allograft mice injected with either control pLKO-ctrl or CXCR4-depleted pLKO-mCXCR4 SMPNST cells) were stained with antibody against BrdU and counterstained with hematoxylin (blue). (D) The percentage of SMPNST cells that were BrdU-positive was determined for each tumor. (E and F) Analysis of the expression levels of various cell cycle genes/proteins in the indicated cells as measured by qPCR (E) and western blotting (F). (G) Cell growth curves of indicated cells as measured with an ATP luminescence assay. (H) CXCR4 and cyclin D1 protein levels were examined by western blotting in indicated cells. Scale bar: 50 um. All statistics represent mean ± SD. (*p< 0.05; **p< 0.01).

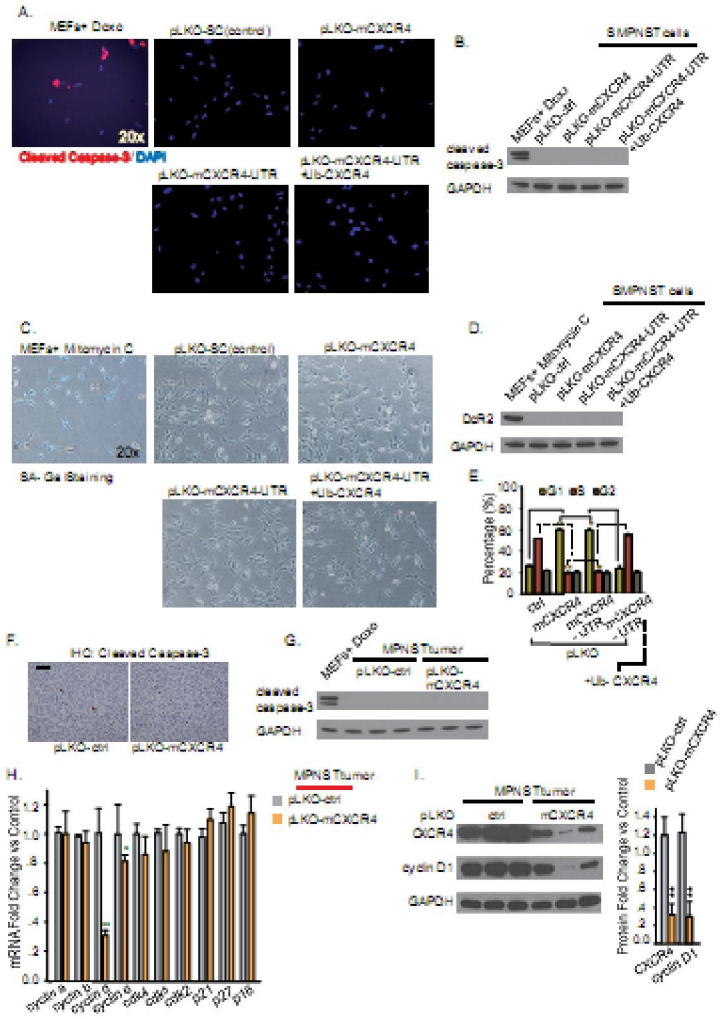

Figure S3. (A) SMPNST cells were stained with antibody against cleaved caspase-3 (red). Cells were counterstained with DAPI (blue), which marks cell nuclei. Wild-type MEFs were treated with doxorubicin as a positive control for apoptotic cell death. (B) Immunoblot of cell lysates from SMPNST cells with antibodies against cleaved caspase-3 (apoptotic marker). (C) SMPNST cells were subjected to SA-Gal staining. (SA=senescence-activated). WT MEFs were treated with mitomycin C as a positive control for senescent cells. (D) Immunoblot of cell lysates from SMPNST cells with antibody against DcR2 (a marker of cell senescence). (E) Quantification of FACS analysis showing percentage of indicated cells in G1, S-phase, or G2. (F) Paraffin sections of MPNSTs (from nude mice injected with either SMPNST cells or CXCR4-depleted SMPNST cells) were stained with antibody against cleaved caspase-3. (G) Immunoblot of tissue lysates from MPNSTs with antibodies against cleaved caspase-3. (H) Analysis of the mRNA levels of various cell cycle genes/proteins in the indicated tumors as measured by qPCR. (I) Western blot with quantification showing decreased CXCR4 and cyclin D1 protein levels in tumors from nude mice (SMPNST-allografts) injected with CXCR4-knockdown MPNST cells. Scale bars: 50 um. All statistics represent mean ± SD. (*p< 0.05; **p< 0.01).

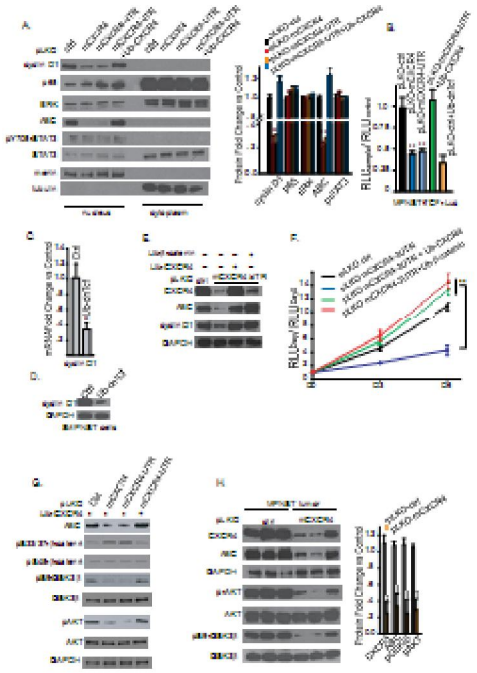

Figure 4. CXCR4 regulates cyclin D1 expression through the AKT/GSK-3β/β-catenin network. (A) Immunoblot of nuclear and cytoplasmic extracts from SMPNST cells with indicated antibodies. (B) Luciferase reporter assay to measure TCF activation in control SMPNST cells (pLKO-ctrl), CXCR4-depleted SMPNST cells (pLKO-mCXCR4, pLKO-mCXCR4-UTR), CXCR4-depleted SMPNST cells rescued by CXCR4 overexpression (pLKO-mCXCR4-UTR+Ub-CXCR4), and SMPNST cells expressing dominant-negative Tcf (pLKO-ctrl+Ub-dnTcf). (C and D) The mRNA and protein levels of cyclin D1 in SMPNST cells (ctrl) or SMPNST cells expressing dnTcf (dnTcf) were determined either by qPCR assay (C) or western blotting (D). (E) Immunoblot of cell lysates from SMPNST cells, CXCR4-depleted SMPNST cells and CXCR4-depleted SMPNST cells ectopically expressing CXCR4 or β-catenin with indicated antibodies (ABC = antibody against activated β-catenin). (F) ATP luminescence assay to measure growth of indicated cells. (G) Immunoblot of cell lysates from SMPNST cells and CXCR4-depleted SMPNST cells with indicated antibodies. (H) Graph showing fold-change versus control of tumor tissue lysates from control SMPNSTs (ctrl) or SMPNSTs from CXCR4-depleted cells (mCXCR4) with indicated antibodies. All statistics represent mean ± SD. (**p< 0.01).

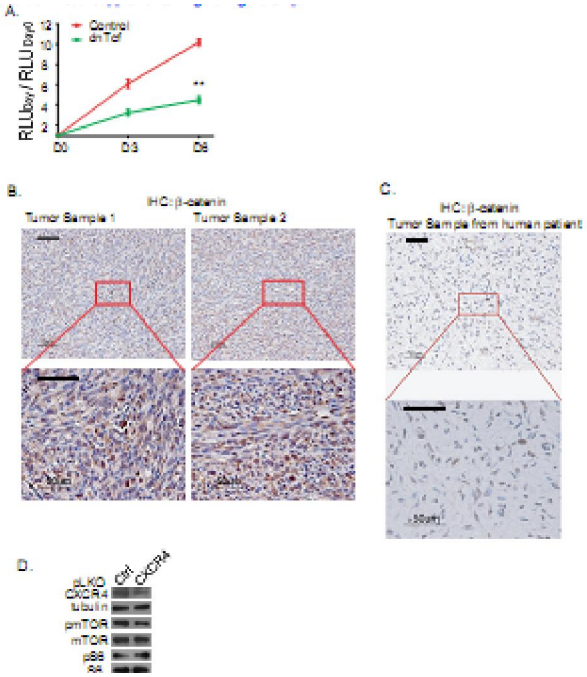

Figure S4 (A) Growth curve of control SMPNST cells or SMPNST cells expressing dominant-negative Tcf (dnTcf) as measured with an ATP luminescence assay. (B and C) Paraffin sections of MPNSTs, either from a mouse model (SMPNST-allografts) (B) or a human NF1 patient (C), were stained with an antibody against -catenin. (D) Immunoblot of cell lysates from control SMPNST cells and CXCR4-depleted SMPNST cells with CXCR4, tubulin, phospho-mTOR, mTOR, phospho-S6 (pS6) and total S6 antibodies. Scale bars: 50 um. All statistics represent mean ± SD. (**p< 0.01).

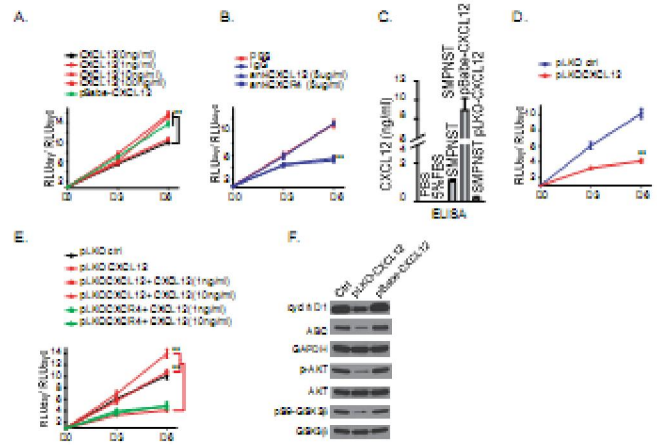

Figure 5. An autocrine mechanism involving CXCL12 and CXCR4 maintains growth of MPNST cells. (A and B) Growth curve of SMPNST cells treated with recombinant CXCL12 protein (A) or CXCL12/CXCR4 antibodies (B). (C) ELISA to measure CXCL12 protein level in PBS, 5% FBS DMEM media, and conditioned media from SMPNST cells or SMPNST cells expressing pBabe-CXCL12 (overexpression) or pLKO-CXCL12 (knockdown). (D) Growth curve of control SMPNST cells (pLKO ctrl) and CXCL12-depleted SMPNST cells (pLKO-CXCL12). (E) Growth curve of SMPNST cells, CXCR4-or CXCL12-depleted SMPNST cells and CXCR4-or CXCL12-depleted SMPNST cells treated with recombinant CXCL12 protein. (F) Immunoblot of cell lysates from SMPNST cells and SMPNST cells expressing pLKO-CXCL12 or pBabe-CXCL12 with indicated antibodies. All statistics represent mean ± SD. (**p< 0.01).

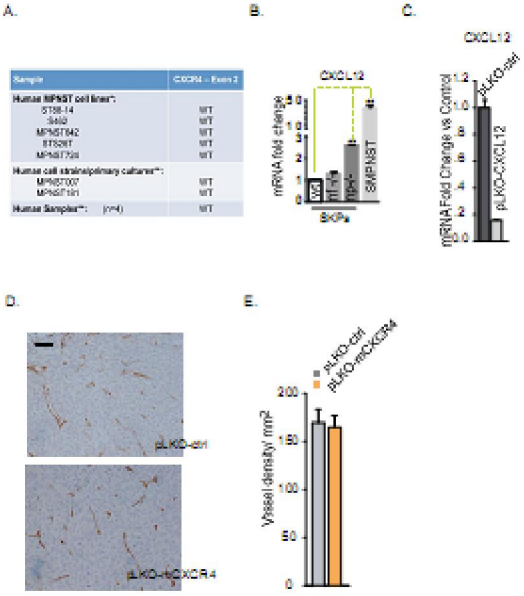

Figure S5. (A) Results of sequence analysis of CXCR4 exon 2 from eleven different human MPNST samples, which included five cell lines, two primary cultures, and four MPNSTs. derived from human patients. (B) qPCR analysis of CXCL12 expression in wild-type, *Nf1*-/-, and *NP*-/- SKPs, and in SMPNST cells. (C) qPCR analysis of CXCL12 mRNA levels in control (pLKO-ctrl) SMPNSTs and CXCL12-knockdown (pLKO-CXCL12) SMPNSTs. (D) Paraffin sections of the indicated SMPNSTs (SMPNST-allografts) were stained with an antibody against CD31. (E) Quantification of vessel density in the indicated tumors. Scale bars: 50 um. All statistics represent mean ± SD. (**p< 0.01).

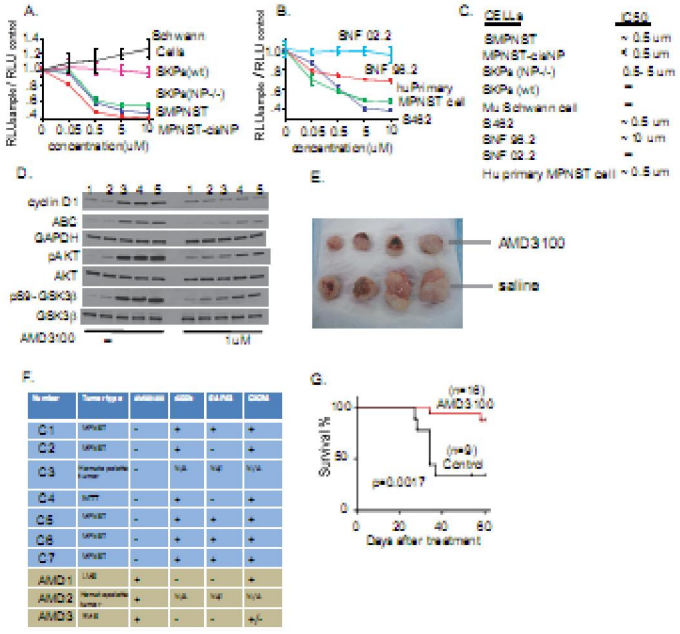

Figure 6. AMD3100 specifically inhibits the proliferation of SMPNST cells and suppresses the growth of MPNSTs in vivo. (A and B) Dose curve showing effect of AMD3100 on proliferation of murine (primary cells from MPNST SKP model and cis*NP* model) and human (SNF 02.2, SNF 96.2, S462 and primary cells from a human NF1 patient) MPNST cells, pre-tumor SKP *NP*-/-cells and WT murine Schwann cells and SKPs. (C) Experimentally-derived AMD3100 IC50 values. (D) Immunoblot with the indicated antibodies of cell lysates from murine cells in the absence or presence of AMD3100. (E) Representative picture of the SMPNST-allograft tumors (from nude mice injected with SMPNST cells) during the treatment study, with tumor histopathology and immunohistochemistry. (G) Kaplan-Meier survival curve of mice in the AMD3100 treatment study (control group, n=9; AMD3100-treated group, n=16; p=0.0017 by Mantel-Cox test). Other statistics represent mean ± SD.

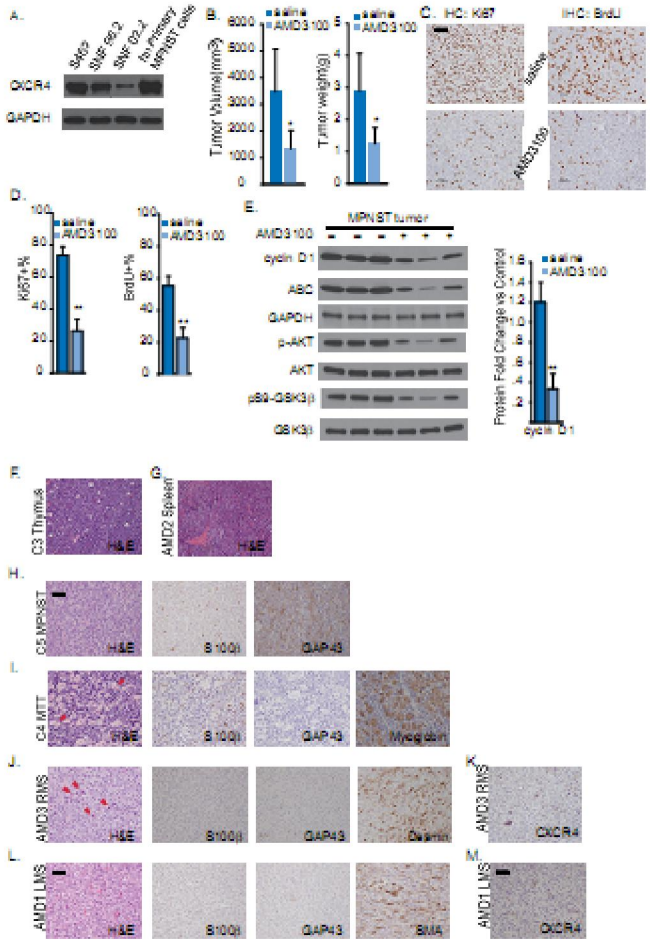

Figure S6 (A) Immunoblot of cell lysates from human MPNST cell lines with CXCR4 antibody. (B) Quantification of MPNST size and weight with (n=6) or without (n=6) AMD3100 treatment. (C) Paraffin sections of SMPNSTs, treated with either saline or AMD3100, were stained with antibody against Ki67 (left panels) and BrdU (right panels). (D) Quantification of the percentage of Ki67-positive cells (left graph) and the percentage of BrdU-positive cells (right graph) in tumors. (E) Immunoblot with indicated antibodies of MPNST tissue lysates from mice treated with or without AMD3100, with quantification of fold change in cyclin D1 protein expression. (F) Hematopoietic tumor in control group. H&E of Thymus. (G) Hematopoietic tumor in experimental group. H&E staining of spleen. (H, I, J and L) Representative pictures of histopathology of the GEMM tumors in control and experimental groups. (H) MPNST- Control group. H&E: typical intersecting fascicles of spindle-shaped cells. IHC: S100 nuclear protein and GAP43 immunoreactivity. (I) MTT (malignant triton tumor) - Control group. H&E: Rhabdomyoblastic cells (arrow) with abundant eosinophilic cytoplasm. IHC; strong immunoreactivity to myoglobin. (J) RMS (rhabdomyosarcoma)- Experimental group. H&E: pleomorphic rhabdomyoblasts (arrow) intermingled with small polygonal cells. IHC: Desmin immunolabels mostly rhabdomyoblasts. (L) LMS (leiomyosarcoma) - Experimental group. Robust -actin (SMA) immunostaining. (K and M). CXCR4 staining of RMS (K) and LMS (M) tumor sections from experimental group. Scale bar: 50 um. All statistics represent mean ± SD. (*p< 0.05; **p< 0.01).

A.

	CXCR4 Intensity			CXCR4 Distribution		
	0	1	2	0	1	2
Neurofibroma (n=17)	1 (6%)	9 (53%)	7 (41%)	5 (29%)	7 (41%)	5 (30%)
NF1-MPNST (n=43)	1 (2%)	33 (77%)	9 (21%)	10 (23%)	15 (35%)	18 (42%)
Sporadic MPNST (n=30)	10 (33%)	16 (53%)	4 (13%)	18 (60%)	8 (27%)	4 (13%)

B.

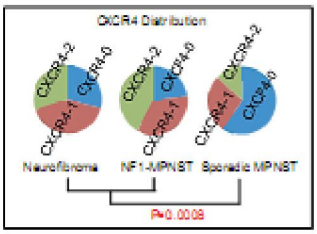

C.

	CXCR4 %	p-AKT %	β-catin intensity	Cyclin D1 %
Correlation coefficient	1	0.362802554	0.447397261	0.558450893
valid cases	43	41	42	40
one-sided significance	0	0.009851018	0.001485903	2.62895E-05

* p-value by 2 for two-sided

D.

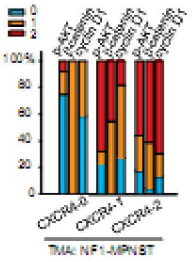

Figure 7. (A) Quantification of the intensity and distribution of CXCR4 immunoreactive cells in all MPNST tissue microarrays (TMAs). (B) Schema of the CXCR4 distribution in TMAs. Spearman correlation identified a statistically significant difference between NF1-associated and sporadic tumors (p=0.0008). (C) Spearman correlation coefficient analyses between CXCR4, pAKT, β-catenin and cyclin D1 in NF1-MPNST. (D) Quantification of pAKT, β-catenin, and cyclin D1 expression levels in MPNST-NF1 TMA, and categorization based on CXCR4 expression level. Staining distribution of positively staining cells: (0) = <5%, (1) = 5-30%, (2) >30%), and intensity: (0) = negative, (1) = low, and (2) = intermediate to high. Spearman's correlation coefficient analyses were used to determine the concordance between CXCR4 expression and NF1 status, and between CXCR4 and other biomarkers.

Conclusion

We took advantage of physiologically relevant mouse modeling to compare the transcriptome of primary NF1-associated MPNST with the cell of origin of the tumor as well as with intermediate pre-tumorigenic cells. The data revealed a progressive increment in expression of the G protein-coupled cytokine receptor CXCR4. We assessed the expression of CXCR4 in additional models of MPNST, as well as in a primary human NF1-associated MPNST and observed similar high expression. Using shRNA and inducible shRNA we knocked down the receptor, its ligand, and putative signaling intermediates that permitted elucidation of a novel mechanism. The study revealed a regulation of cyclin D1, and thus cell cycle progression, by CXCR4 via, PI3K, GSK-3beta/ beta-catenin, and TCF. This biochemical pathway was validated by successive knockdown of intermediates and expression of downstream effectors using mouse and human MPNST cells. Furthermore we demonstrated a novel autocrine loop wherein CXCL12, the physiological ligand, is produced by the tumor cells. Tumor allografts were employed to demonstrate that knockdown, inducible knockdown, and pharmacological inhibition of CXCR4, blunted tumor development and concomitantly blocked all the pathway intermediates described

above. Finally, human tumor microarrays validated CXCR4 expression in a large majority of tumors and further demonstrated a conservation of the activated pathway elucidated in the mouse system. We have further demonstrated that like its receptor, CXCL12 levels are substantially elevated in NF1 malignant cells. Thus, there is an amplification of the autocrine loop and the tumor cells are addicted to the supply. Finally, we perform preclinical evaluation of AMD3100, a specific CXCR4 inhibitor, on a spontaneous MPNST GEMM. The data are clear and demonstrate a robust and incontrovertible inhibition of solid tumor development in the treated mice.

References

Balkwill, F. (2004). The significance of cancer cell expression of the chemokine receptor CXCR4. Semin Cancer Biol *14*, 171-179.

Bertolini, F., Dell'Agnola, C., Mancuso, P., Rabascio, C., Burlini, A., Monestiroli, S., Gobbi, A., Pruneri, G., and Martinelli, G. (2002). CXCR4 neutralization, a novel therapeutic approach for non-Hodgkin's lymphoma. Cancer Res *62*, 3106-3112.

Bian, X.W., Yang, S.X., Chen, J.H., Ping, Y.F., Zhou, X.D., Wang, Q.L., Jiang, X.F., Gong, W., Xiao, H.L., Du, L.L.*, et al.* (2007). Preferential expression of chemokine receptor CXCR4 by highly malignant human gliomas and its association with poor patient survival. Neurosurgery *61*, 570-578; discussion 578-579.

Burger, J.A., Burger, M., and Kipps, T.J. (1999). Chronic lymphocytic leukemia B cells express functional CXCR4 chemokine receptors that mediate spontaneous migration beneath bone marrow stromal cells. Blood *94*, 3658-3667.

Cichowski, K., Shih, T.S., Schmitt, E., Santiago, S., Reilly, K., McLaughlin, M.E., Bronson, R.T., and Jacks, T. (1999). Mouse models of tumor development in neurofibromatosis type 1. Science *286*, 2172-2176.

Cross, D.A., Alessi, D.R., Cohen, P., Andjelkovich, M., and Hemmings, B.A. (1995). Inhibition of glycogen synthase kinase-3 by insulin mediated by protein kinase B. Nature *378*, 785-789.

Cui, Y., Costa, R.M., Murphy, G.G., Elgersma, Y., Zhu, Y., Gutmann, D.H., Parada, L.F., Mody, I. and Silva, A.J. (2008). Neurofibromin regulation of ERK signaling modulates GABA release and learning. Cell *135*, 549-60.

Ferner, R.E. (2007). Neurofibromatosis 1. Eur J Hum Genet *15*, 131-138.

Ghadimi, M.P., Young, E.D., Belousov, R., Zhang, Y., Lopez, G., Lusby, K., Kivlin, C., Demicco, E.G., Creighton, C.J., Lazar, A.J., *et al.* (2012). Survivin is a viable target for the treatment of malignant peripheral nerve sheath tumors. Clin Cancer Res *18*, 2545-2557.

Hoppler, S., and Kavanagh, C.L. (2007). Wnt signalling: variety at the core. J Cell Sci *120*, 385-393.

Johannessen, C.M., Johnson, B.W., Williams, S.M., Chan, A.W., Reczek, E.E., Lynch, R.C., Rioth, M.J., McClatchey, A., Ryeom, S., and Cichowski, K. (2008). TORC1 is essential for NF1-associated malignancies. Curr Biol *18*, 56-62.

Johansson, G., Mahller, Y.Y., Collins, M.H., Kim, M.O., Nobukuni, T., Perentesis, J., Cripe, T.P., Lane, H.A., Kozma, S.C., Thomas, G., *et al.* (2008). Effective in vivo targeting of the mammalian target of rapamycin pathway in malignant peripheral nerve sheath tumors. Mol Cancer Ther *7*, 1237-1245.

Johnson, D.G., and Walker, C.L. (1999). Cyclins and cell cycle checkpoints. Annu Rev Pharmacol Toxicol *39*, 295-312.

Joseph, N.M., Mosher, J.T., Buchstaller, J., Snider, P., McKeever, P.E., Lim, M., Conway, S.J., Parada, L.F., Zhu, Y., and Morrison, S.J. (2008). The loss of Nf1 transiently promotes self-renewal but not tumorigenesis by neural crest stem cells. Cancer Cell *13*, 129-140.

Kijima, T., Maulik, G., Ma, P.C., Tibaldi, E.V., Turner, R.E., Rollins, B., Sattler, M., Johnson, B.E., and Salgia, R. (2002). Regulation of cellular proliferation, cytoskeletal function, and signal transduction through CXCR4 and c-Kit in small cell lung cancer cells. Cancer Res *62*, 6304-6311.

Koshiba, T., Hosotani, R., Miyamoto, Y., Ida, J., Tsuji, S., Nakajima, S., Kawaguchi, M., Kobayashi, H., Doi, R., Hori, T., *et al.* (2000). Expression of stromal cell-derived factor 1 and CXCR4 ligand receptor system in pancreatic cancer: a possible role for tumor progression. Clin Cancer Res *6*, 3530-3535.

Laverdiere, C., Hoang, B.H., Yang, R., Sowers, R., Qin, J., Meyers, P.A., Huvos, A.G., Healey, J.H., and Gorlick, R. (2005). Messenger RNA expression levels of CXCR4 correlate with metastatic behavior and outcome in patients with osteosarcoma. Clin Cancer Res *11*, 2561-2567.

Le, L.Q. and Parada, L.F. (2007). Tumor microenvironment and neurofibromatosis type I: connecting the GAPs. Oncogene *26*, 4609-4616.

Le, L.Q., Liu, C., Shipman, T., Chen, Z., Suter, U., and Parada, L.F. (2011). Susceptible stages in Schwann cells for NF1-associated plexiform neurofibroma development. Cancer Res *71*, 4686-4695.

Le, L.Q., Shipman, T., Burns, D.K., and Parada, L.F. (2009). Cell of origin and microenvironment contribution for NF1-associated dermal neurofibromas. Cell Stem Cell *4*, 453-463.

Lee, M.H., and Yang, H.Y. (2003). Regulators of G1 cyclin-dependent kinases and cancers. Cancer Metastasis Rev *22*, 435-449.

Li, Y.M., Pan, Y., Wei, Y., Cheng, X., Zhou, B.P., Tan, M., Zhou, X., Xia, W., Hortobagyi, G.N., Yu, D.*, et al.* (2004). Upregulation of CXCR4 is essential for HER2-mediated tumor metastasis. Cancer Cell *6*, 459-469.

Liu, C., Li, Y., Semenov, M., Han, C., Baeg, G.H., Tan, Y., Zhang, Z., Lin, X., and He, X. (2002). Control of beta-catenin phosphorylation/degradation by a dual-kinase mechanism. Cell *108*, 837-847.

Mantripragada, K.K., Spurlock, G., Kluwe, L., Chuzhanova, N., Ferner, R.E., Frayling, I.M., Dumanski, J.P., Guha, A., Mautner, V., and Upadhyaya, M. (2008). High-resolution DNA copy number profiling of malignant peripheral nerve sheath tumors using targeted microarray-based comparative genomic hybridization. Clin Cancer Res *14*, 1015-1024.

Muller, A., Homey, B., Soto, H., Ge, N., Catron, D., Buchanan, M.E., McClanahan, T., Murphy, E., Yuan, W., Wagner, S.N.*, et al.* (2001). Involvement of chemokine receptors in breast cancer metastasis. Nature *410*, 50-56.

Obaya, A.J., and Sedivy, J.M. (2002). Regulation of cyclin-Cdk activity in mammalian cells. Cell Mol Life Sci *59*, 126-142.

Oh, J.W., Drabik, K., Kutsch, O., Choi, C., Tousson, A., and Benveniste, E.N. (2001). CXC chemokine receptor 4 expression and function in human astroglioma cells. J Immunol *166*, 2695-2704.

Peled, A., Wald, O., and Burger, J. (2012). Development of novel CXCR4-based therapeutics. Expert Opin Investig Drugs *21*, 341-353.

Righi, E., Kashiwagi, S., Yuan, J., Santosuosso, M., Leblanc, P., Ingraham, R., Forbes, B., Edelblute, B., Collette, B., Xing, D.*, et al.* (2011). CXCL12/CXCR4 blockade induces multimodal antitumor effects that prolong survival in an immunocompetent mouse model of ovarian cancer. Cancer Res *71*, 5522-5534.

Rubin, J.B., and Gutmann, D.H. (2005). Neurofibromatosis type 1 -a model for nervous system tumour formation? Nat Rev Cancer *5*, 557-564.

Schrader, A.J., Lechner, O., Templin, M., Dittmar, K.E., Machtens, S., Mengel, M., Probst-Kepper, M., Franzke, A., Wollensak, T., Gatzlaff, P.*, et al.* (2002). CXCR4/CXCL12 expression and signalling in kidney cancer. Br J Cancer *86*, 1250-1256.

Sehgal, A., Keener, C., Boynton, A.L., Warrick, J., and Murphy, G.P. (1998). CXCR-4, a chemokine receptor, is overexpressed in and required for proliferation of glioblastoma tumor cells. J Surg Oncol *69*, 99-104.

Sengupta, R., Dubuc, A., Ward, S., Yang, L., Northcott, P., Woerner, B.M., Kroll, K., Luo, J., Taylor, M.D., Wechsler-Reya, R.J., *et al.* (2011). CXCR4 activation defines a new subgroup of Sonic hedgehog-driven medulloblastoma. Cancer Res *72*, 122-132.

Serra, E., Rosenbaum, T., Winner, U., Aledo, R., Ars, E., Estivill, X., Lenard, H.G., and Lazaro, C. (2000). Schwann cells harbor the somatic NF1 mutation in neurofibromas: evidence of two different Schwann cell subpopulations. Hum Mol Genet *9*, 3055-3064.

Sherr, C.J. (1995). D-type cyclins. Trends Biochem Sci *20*, 187-190.

Singh, S., Singh, U.P., Grizzle, W.E., and Lillard, J.W., Jr. (2004). CXCL12-CXCR4 interactions modulate prostate cancer cell migration, metalloproteinase expression and invasion. Lab Invest *84*, 1666-1676.

Srivastava, A.K., and Pandey, S.K. (1998). Potential mechanism(s) involved in the regulation of glycogen synthesis by insulin. Mol Cell Biochem *182*, 135-141.

Szudek, J., Birch, P., Riccardi, V.M., Evans, D.G., and Friedman, J.M. (2000). Associations of clinical features in neurofibromatosis 1 (NF1). Genet Epidemiol *19*, 429-439.

Taichman, R.S., Cooper, C., Keller, E.T., Pienta, K.J., Taichman, N.S., and McCauley,

L.K. (2002). Use of the stromal cell-derived factor-1/CXCR4 pathway in prostate cancer metastasis to bone. Cancer Res *62*, 1832-1837.

Tonsgard, J.H. (2006). Clinical manifestations and management of neurofibromatosis type 1. Semin Pediatr Neurol *13*, 2-7.

Vogel, K.S., Klesse, L.J., Velasco-Miguel, S., Meyers, K., Rushing, E.J., and Parada, L.F. (1999). Mouse tumor model for neurofibromatosis type 1. Science *286*, 2176-2179.

Wang, Z., Ma, Q., Liu, Q., Yu, H., Zhao, L., Shen, S., and Yao, J. (2008). Blockade of SDF-1/CXCR4 signalling inhibits pancreatic cancer progression in vitro via inactivation of canonical Wnt pathway. Br J Cancer *99*, 1695-1703.

Wang, Y., Kim, E., Wang, X., Novitch, B.G., Yoshikawa, K., Chang, L.S. and Zhu, Y. (2012). ERK inhibition rescues defects in fate specification of Nf1-deficient neural progenitors and brain abnormalities. Cell *150*, 816-30.

Warrington, N.M., Woerner, B.M., Daginakatte, G.C., Dasgupta, B., Perry, A., Gutmann, D.H., and Rubin, J.B. (2007). Spatiotemporal differences in CXCL12 expression and cyclic AMP underlie the unique pattern of optic glioma growth in neurofibromatosis type Cancer Res *67*, 8588-8595.

Zeelenberg, I.S., Ruuls-Van Stalle, L., and Roos, E. (2003). The chemokine receptor CXCR4 is required for outgrowth of colon carcinoma micrometastases. Cancer Res *63*, 3833-3839.

Zheng, H., Chang, L., Patel, N., Yang, J., Lowe, L., Burns, D.K., and Zhu, Y. (2008). Induction of abnormal proliferation by nonmyelinating schwann cells triggers neurofibroma formation. Cancer Cell *13*, 117-128.

Zhou, Y., Larsen, P.H., Hao, C., and Yong, V.W. (2002). CXCR4 is a major chemokine receptor on glioma cells and mediates their survival. J Biol Chem *277*, 49481-49487.

Zhu, Y. and Parada, L.F. (2001). Neurofibromin, a tumor suppressor of the nervous system. Exp. Cell Research *264*,19-28.

Zhu, Y., Ghosh, P., Charnay, P., Burns, D.K., and Parada, L.F. (2002). Neurofibromas in NF1: Schwann cell origin and role of tumor environment. Science *296*, 920-922.

Zou, C.Y., Smith, K.D., Zhu, Q.S., Liu, J., McCutcheon, I.E., Slopis, J.M., Meric-Bernstam, F., Peng, Z., Bornmann, W.G., Mills, G.B.*, et al.* (2009). Dual targeting of AKT and mammalian target of rapamycin: a potential therapeutic approach for malignant peripheral nerve sheath tumor. Mol Cancer Ther *8*, 1157-1168.

Appendices

MPNST: malignant peripheral nerve sheath tumors
SKPs: skin-derived progenitors
GPCR: G protein-coupled seven-transmembrane receptor
IHC: immunhistochemistry
NP: NF1 and TP53